volume to 25 mL with 0.067 mol/L phosphate buffer, pH 6.8. The entire 25-mL volume was injected into a valve body using a programmable syringe drive. The filtered samples were washed with 5 mL of water and then lysed for ~ 20 s. After the lysis step, the material was forced through the filter by air pressure, and PCR was performed on aliquots of the filtered lysate. Typically, 100 μL of filtered lysate was recovered.

All real-time fluorescence (RTF)-PCR reactions were performed using Cepheid SmartCycler® instrumentation and reaction tubes. The Mtb-specific primers and 6-carboxyfluorescein-labeled Molecular Beacon probes are described elsewhere (El-Hajj H, Marras SA, Tyagi S, Kramer FR, Alland D. A multiplex multi-colored Molecular Beacon assay for the rapid identification of *Mycobacterium tuberculosis* and rifampin resistance in clinical sputum samples, manuscript in preparation). Thermocycling conditions were 2 min at 95 °C, followed by 50 cycles of 10 s at 95 °C, 15 s at 58 °C, and 10 s at 72 °C. Fluorescence was measured during the 58 °C steps.

RTF-PCR results demonstrated the effectiveness of ultrasonic lysis for rupturing the BCG in the tube lysis system. When we used 10-fold serial dilutions of cultured cells, 14 CFU/100-μL aliquot were detected. This demonstrated that ultrasonic lysis with silica beads was effective on BCG cells.

Serial 10-fold dilutions of BCG from 1480 to 0.015 CFU/mL were processed using the one-piece valve body and then analyzed by RTF-PCR.

The results for several of the samples, tested in duplicate, are shown in Fig. 1. Sample 1 is purified Mtb DNA (single result), sample 2 is 148 CFU/mL, sample 3 is 14.8 CFU/mL, and sample 6 is 0.015 CFU/mL. Samples with <14.8 CFU/mL were not detected in this series of experiments. Control experiments showed that ultrasonic lysis was required for DNA detection and that the NaOH solution was PCR-inhibitory.

These data from experiments using prototype filtration/lysis devices demonstrate the sample processing capabilities of the valve body component of the GeneXpert cartridge. The system effectively lyses BCG by use of ultrasonic energy and concentrates dilute, large volume samples by filtration. An additional advantage of the system is the ability to remove inhibitors of PCR by washing the captured sample. Removal of inhibitors will allow the use of current sputum digestant reagents, which will be important for comparison studies with culture and acid-fast bacteria staining methods of Mtb detection. The valve body is also capable of handling small or large sample volumes. These qualities are important for the range of applications planned for this system.

Release of detectable amounts of DNA without lysis was not observed. This implies that the system can concentrate and wash intact organisms, efficiently concentrating the target DNA after a subsequent lysis step. On the basis of the CFU calculations, a titer not detectable by PCR was concentrated to easily detectable concentrations.

Future efforts will investigate areas important for analytical sensitivity and user requirements of rapid detection. Such areas will include filter surface area, pore size and material, valve body contained volume, fluid pumping rates, buffer composition, and ultrasonic lysis conditions, and other variables.

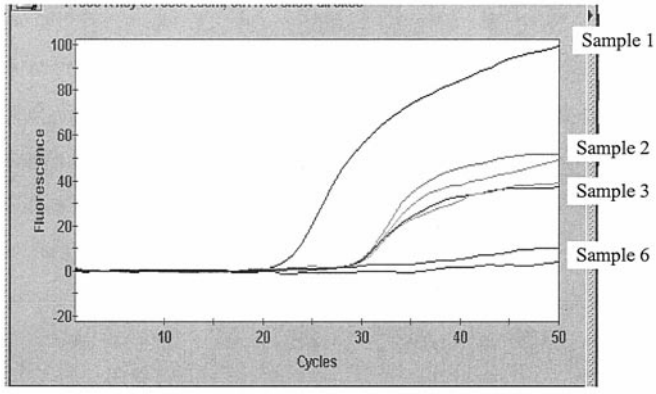

Fig. 1. RTF results for purified Mtb DNA (*Sample 1*), 148 CFU/mL BCG (*Sample 2*), 14.8 CFU/mL BCG (*Sample 3*), and 0.015 CFU/mL BCG (*Sample 6*).

Finally, currently developed RTF multiplex PCR assays for Mtb single-nucleotide polymorphisms important in rifampin drug resistance will be adapted to the GeneXpert system. This may provide the final, critical technologic capability for the rapid, simultaneous, sensitive detection of Mtb and the presence of antibiotic resistance.

Technical assistance was provided by Molly Miranda, Rick Faeth, and Kristen Lloyd.

Magnetic Resonance Diagnostics: A New Technology for High-Throughput Clinical Diagnostics, *David S. Wishart,[1] Lori M.M. Querengesser,[2*] Brent A. Lefebvre,[2] Noah A. Epstein,[2] Russ Greiner,[3] and Jack B. Newton[2]* ([1] 2123 Dentistry/Pharmacy Center, Faculty of Pharmacy and Pharmaceutical Sciences, University of Alberta, Edmonton, Alberta, T6G 2N8 Canada; [2] Chenomx Inc., 2007, 8308-114 Street, Edmonton, Alberta, T6G 2E1 Canada; [3] 122 Athabasca Hall, Artificial Intelligence Group, Department of Computing Science, University of Alberta, Edmonton, Alberta, T6G 2E8 Canada; * author for correspondence: fax 780-432-3388, e-mail lquerengesser@chenomx.com)

Magnetic resonance diagnostics (MRD) uses automated, high-throughput nuclear magnetic resonance (NMR) spectroscopy for the rapid identification and quantification of small-molecule metabolites in biofluid mixtures (blood, urine, saliva, cerebrospinal fluid, and others). Specifically, MRD involves using a high-field (400 MHz) NMR instrument equipped with a small-volume flow

probe and robotic sample handler to rapidly load biofluid samples and to collect their ^{1}H NMR spectra. Spectral deconvolution software automatically assigns individual peaks to particular compounds and calculates concentrations from peak areas. MRD uses the principle of chemical shift separation to physically separate and identify individual compounds directly from ^{1}H NMR spectra, thus avoiding chromatographic separation steps (e.g., HPLC, gas chromatography, and capillary electrophoresis). MRD is useful for rapid (<2 min per sample) qualitative and quantitative assessment of small-molecule metabolites.

NMR spectroscopy is not new to the field of clinical chemistry. Indeed several important applications have already been demonstrated in the area of diagnosis and therapeutic monitoring of metabolic disorders *(1–4)*, in toxicologic and renal testing *(5*, *6)*, and in the profiling of blood lipoproteins and cholesterol *(7)*. An emerging approach to enable high-throughput in vivo toxicology is called metabonomics, which uses high-resolution NMR to rapidly evaluate the metabolic status of an animal *(8*, *9)*.

A key limitation to all of these NMR approaches is that they depend on manual sample handling and/or manual (i.e., expert) spectral analysis. This has made most NMR approaches to clinical analyses far too slow or too costly for routine chemical profiling or high-throughput screening. Because MRD is fully automated (sample handling, spectral collection, and spectral analysis are all handled by robots or computers), this technique offers the potential for high-throughput, comprehensive, and inexpensive chemical analysis of a wide range of biofluid samples.

To demonstrate the potential of MRD for high-throughput clinical screening and metabolic profiling, we constructed a simulated test-run of 1000 urine samples processed by a prototype MRD instrument developed jointly by our laboratory and Varian Inc. (Palo Alto, CA). Our intent was to investigate the performance of the MRD instrument and software under the demands of a high-throughput clinical testing laboratory. The instrument was assessed on sample-processing speed, robustness of sample handling, and accuracy of identifying samples and compounds.

We followed protocols and conditions approved by the University of Alberta's Health Research Ethics Board to collect 1000 anonymous urine samples. A total of 925 samples were obtained from healthy adult volunteers who had completed consent forms. Seventy-five samples (63 children, 12 adults) were obtained as anonymous "discards" from several hospitals and clinics across Canada and were from patients with a wide variety of inborn errors of metabolism, neuroblastoma, and alcohol poisoning. All of the abnormal samples used in this test had been identified previously as such through conventional clinical screens. Among the abnormal samples were the following: 14 with propionic acidemia; 11 with methylmalonic aciduria; 11 with cystinuria; 6 with alkaptonuria; 4 with glutaric aciduria I; 3 each with pyruvate decarboxylase deficiency, ketosis, Hartnup disorder, cystinosis, neuroblastoma, phenylketonuria, ethanol toxicity, glycerol kinase deficiency, and hydroxymethylglutaryl-CoA-lyase deficiency; and 2 with carbamoylphosphate synthetase deficiency.

For MRD analysis, 990-μL portions from each urine sample were transferred to 1.8-mL autosampler vials, to which 0.5 mmol/L (10 μL of a 50 mmol/L solution) 3-(trimethylsilyl)-1-propane-sulfonic acid, sodium salt (Sigma-Aldrich) was added. We manually adjusted the samples to pH 6.5 using $HCl_{(aq)}$ or $NaOH_{(aq)}$, as necessary. Manual pH adjustment was necessary because the software module required to automatically measure the pH and adjust the spectral deconvolution process was not completed in time for this study.

The prototype MRD instrument consisted of a 400 MHz Varian NMR spectrometer equipped with a 60-μL triple resonance-flow probe with an interchangeable flow cell and a modified Varian VAST (Versatile Automatic Sample Transport) system. The VAST system uses a robotic liquid handler (Gilson Model 215) and three computer-controlled switching valves, which direct sample flow to and from the flow probe through small-diameter Teflon tubing. Each urine sample (250 μL) was automatically loaded into the NMR spectrometer and a one-dimensional ^{1}H NMR spectrum collected (12 scans, 1.998 s; acquisition time, 0.5 s; acquisition delay, 6000 Hz sweepwidth) at ambient temperature (21.5 °C ± 0.5 °C). After data collection, the urine sample was ejected and the flow probe extensively rinsed with distilled water before the next sample was loaded. Sample carryover was <1%.

NMR spectra were autoprocessed (e.g., transformed, phased, and referenced) and deconvolved with a suite of specially developed software applications and databases. The deconvolution process allows for the automated identification and quantification of components in biofluid mixtures through spectral database comparisons. We tested for 149 compounds currently contained in our spectral database.

The instrument automatically loaded and analyzed all 1000 samples in 35.2 h (1 sample every 2.1 min) with minimal human supervision. The mean sample loading and rinsing time was 93 s, whereas spectral acquisition had a mean of 32 s. The mean times for spectral processing and deconvolution (which can be performed in parallel with sample loading and data acquisition) were 7.1 and 72 s, respectively. During the test run, one sample-loading failure occurred, but did not lead to instrument downtime.

The deconvolution software was tested for accuracy for the following: (*a*) identification and quantification of urinary metabolites, (*b*) identification of nonpathologic and abnormal urine samples, and (*c*) identification of specific disease states or conditions. We evaluated compound-identification and/or -quantification accuracy primarily through detailed analysis of the abnormal samples. Specifically, the 15 disorders found in the abnormal urine samples were characterized by 34 unique or abnormally abundant metabolites (e.g., homogentisic acid, glycerol, glutaric acid, and others). Our results indicate that the MRD software succeeded in correctly identifying all 34 abnormal metabolites in all 75 abnormal samples. All 34

metabolites had been identified previously through conventional HPLC, gas chromatography–mass spectrometry, or amino acid or organic acid analysis. In some cases, these metabolites were also detected in nonpathologic urine samples, but at concentrations too low to be of significance or at concentrations well within the reference interval *(10)*.

Although it was not possible to verify the MRD-measured concentrations for all metabolites (most conventional tests provide only qualitative results), our results for those metabolites that could be reliably quantified indicated a correlation coefficient between conventionally measured concentrations and MRD-measured concentrations of 0.99 (spanning a concentration range of 400 μmol/L to 550 mmol/L). An example of compound identification and quantification achieved by this MRD software is shown in Fig. 1, which shows an abnormal urine NMR spectrum (specifically, methylmalonic aciduria), along with the MRD-calculated NMR spectrum. The calculated spectrum was generated from individual NMR spectra of MRD-identified and -quantified compounds.

Among nonpathologic urine samples, 87 $\pm$ 11 compounds were routinely identified and quantified by the MRD software on average. The identification and concentration of these metabolites were partially verified through manual spectral analysis of three randomly chosen samples and their subsequent chemical analysis. It was not practical to attempt to verify the identity of all compounds in the nonpathologic urine samples via conventional assays. The MRD software failed to consistently identify citrate, glycine, and histidine, probably because of the extreme sensitivity of their chemical shifts to pH and/or calcium ion concentrations.

A simple concentration-threshold algorithm achieved 96% sensitivity and 100% specificity, with 72 of 75 abnormal samples being detected and all 925 nonpathologic samples being correctly classified as nonpathologic. The three missed abnormal samples were cystinuria, glutaric aciduria, and carbamoylphosphate synthetase deficiency. This misclassification arose from the fact that these three samples exhibited relatively modest concentrations of abnormal metabolites. This particular algorithm compared MRD-quantified metabolite data with those values reported by Tietz *(10)*, a database of "normal" and "abnormal" metabolite concentrations (both absolute and relative to creatinine) tabulated from several literature sources, as well as metabolite data collected from our own assays. Age- and gender-related adjustments were not included in the classification scheme.

Tests of the disease classification accuracy (for 1 healthy state and 15 diseases or conditions) yielded 95.5% and 92.4% for sensitivity and specificity, respectively. Interestingly, all false positives were confined to those urine samples already classified as abnormal. In particular, four false positives were identified for propionic aciduria, three false positives for phenylketonuria, two false positives were identified for cystinuria, and one false positive for ethanol toxicity. These classification problems likely arose from the age-independent, all-or-none classification scheme used by our algorithm. A probabilistic assessment that included age- or gender-related values would likely have improved the results or revealed multiple disease possibilities.

Overall, this prototype instrument was rapid, robust, and accurate. It rapidly identified and quantified key metabolic markers of both common conditions (ethanol toxicity) and rare disorders (neuroblastoma). It appears to offer a high-throughput, inexpensive approach to metabolic profiling, with possible applications in medical

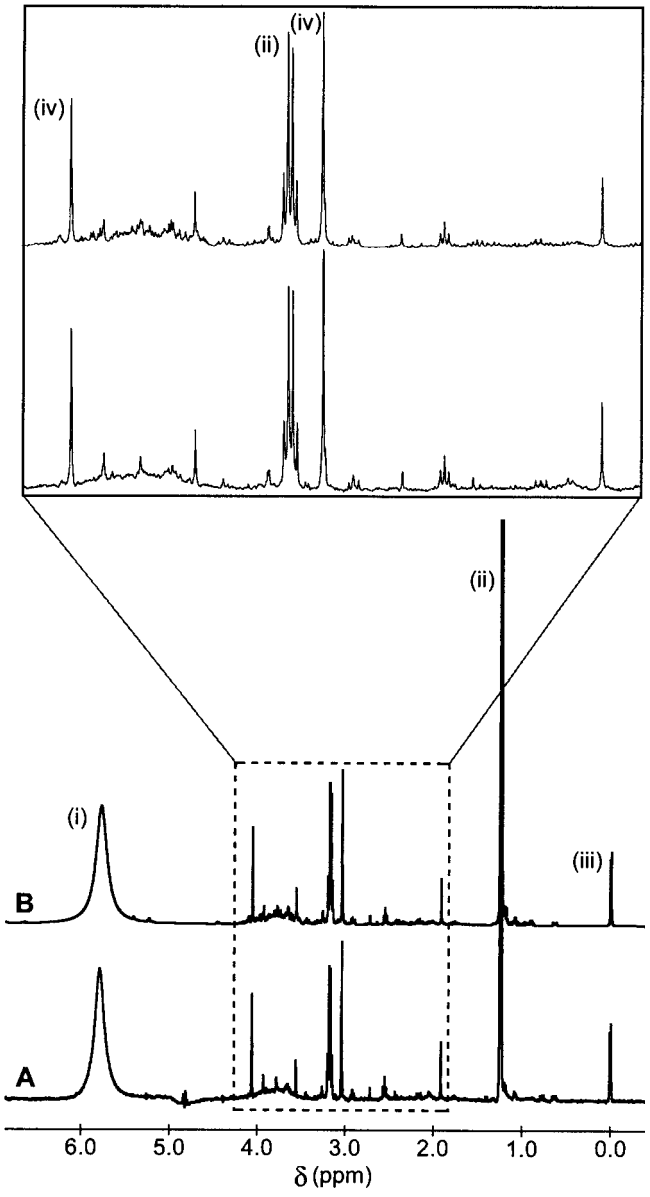

Fig. 1. NMR spectrum compared with software-generated spectrum.

(*A*), ^{1}H NMR spectrum of a urine sample from a patient with methylmalonic aciduria. (*B*), calculated NMR spectrum derived from summing the individual spectra of the compounds and concentrations determined by the MRD software. (*Inset*), an enlargement of the region between 1.9 and 4.1 ppm. Peak labels are as follows: *(i)*, urea; *(ii)*, 2-methyl malonate; *(iii)*, 2,2-dimethyl-2-silapentanesulfonic acid; *(iv)*, creatinine.

diagnostics, drug compliance testing, toxicology, and food testing.

We wish to thank the University of Alberta Hospital, Toronto Hospital for Sick Children, Children's & Women's Health Centre of British Columbia, and Health Sciences Centre (Winnipeg, Manitoba) for contributing samples for this study. We also thank Dr. Fiona Bamforth (Department of Laboratory Medicine and Pathology, University of Alberta) for invaluable advice.

References

1. Lindon JC, Nicholson JK, Everett JR. NMR Spectroscopy of Biofluids. Annu Rep NMR Spectrosc 1999;38:1–88.
2. Wevers RA, Engelke UFH, Moolenaar SH, Brautigam C, De Jong JGN, Duran R, et al. ^{1}H-NMR spectroscopy of body fluids: inborn errors of purine and pyrimidine metabolism. Clin Chem 1999;45:539–48.
3. Bamforth FJ, Dorian V, Vallance H, Wishart DS. Diagnosis of inborn errors of metabolism using ^{1}H NMR spectroscopic analysis of urine. J Inherit Metab Dis 1999;22:297–301.
4. Burns SP, Woolf DA, Leonard JV, Iles RA. Investigation of urea cycle enzyme disorders by ^{1}H-NMR spectroscopy. Clin Chim Acta 1992;209:47–60.
5. Komoroski E M, Komoroski RA, Valentine JL, Pearce JM, Kearns GL. The use of nuclear magnetic resonance spectroscopy in the detection of drug intoxication. J Anal Toxicol 2000;24:180–7.
6. Foxall PJD, Mellotte GJ, Bending MR, Lindon JC, Nicholson JK. NMR spectroscopy as a novel approach to the monitoring of renal transplant function. Kidney Int 1993;43:234–45.
7. Freedman DS, Otvos JD, Jeyarajah EJ, Barboriak JJ, Anderson AJ, Walker JA. Relation of lipoprotein subclasses as measured by proton nuclear magnetic resonance spectroscopy to coronary artery disease. Arterioscler Thromb Vasc Biol 1998;18:1046–53.
8. Nicholson JK, Lindon JC, Holmes E. 'Metabonomics': understanding the metabolic responses of living systems to pathophysiological stimuli via multivariate statistical analysis of biological NMR spectroscopic data. Xenobiotica 1999;29:1181–9.
9. Robertson DG, Reily MD, Sigler RE, Wells DF, Paterson DA, Braden TK. Metabonomics: evaluation of nuclear magnetic resonance (NMR) and pattern recognition technology for rapid in vivo screening of liver and kidney toxicants. Toxicol Sci 2000;57:326–37.
10. Tietz, NW, ed. Clinical guide to laboratory tests, 3rd ed. Philadelphia: WB Sanders Press, 1995:1–760.

The Use of Inosine 5′-Monophosphate Dehydrogenase (IMPDH) in the Development of a New Liquid Homogeneous Enzyme Immunoassay Technology, *Allan R. Dorn,* Larry D. Mountain, Mitali Ghoshal, Raymond A. Hui, Lisa K. Klinedinst, Janice E. Rugaber, Andrew F. Schamerloh, and Salvatore J. Salamone* (Roche Diagnostics Corporation, Centralized Diagnostics Business Unit, 9115 Hague Rd., PO Box 50457, Indianapolis, IN 46250-0457; * author for correspondence: fax 317-521-3085, e-mail allan.dorn@roche.com)

The objective of the present study was the development of a quantitative liquid homogeneous immunoassay specific for theophylline based on the specific uncompetitive inhibition of inosine 5′-monophosphate dehydrogenase (IMPDH) by mycophenolic acid (MPA). This was accomplished by covalent coupling of theophylline to MPA to form a theophylline-MPA conjugate (Fig. 1).

IMPDH (EC 1.1.1.205) *(1)* catalyzes the NAD-dependent oxidation of inosine 5′-monophosphate (IMP) to xanthosine 5′-monophosphate (XMP). The enzyme follows an ordered Bi-Bi reaction sequence of substrate and cofactor binding and product release. In the first step, IMP binds to IMPDH, followed by the binding of the cofactor NAD. After IMP oxidation, the reduced cofactor, NADH, is released from IMPDH, followed by the release of XMP. To monitor the reaction, the rate of NADH formation is measured at 340 nm. Uncompetitive inhibition occurs when MPA combines with the IMPDH-XMP complex at the active site of the enzyme to form IMPDH-XMP-MPA complex, which is unable to release XMP. IMPDH inhibition depends only on the concentration of MPA because of the uncompetitive nature of inhibition by MPA. Thus, the greater the concentration of MPA inhibitor, the greater the inhibition of the enzyme. An uncompetitive inhibitor of IMPDH inhibits by binding at the active site of the enzyme and does not compete with IMP or NAD for inhibition of the enzyme. Increasing substrate concentration does not reverse this type of inhibition.

Two properties of MPA inhibition of IMPDH may facilitate the development of homogeneous enzyme immunoassays. The first property is that an uncompetitive inhibitor as a target conjugate is preferred over a competitive inhibitor because uncompetitive inhibitors are rare in nature and should be less susceptible to interferences from drugs and naturally occurring substances, which frequently are competitive inhibitors of enzymes. The second property is that the sensitivity of MPA inhibition (K_i = 10 nmol/L) *(2)* favors its use in enzyme immunoassays.

We developed this homogeneous immunoassay by covalently attaching theophylline to a position on MPA that did not interfere with the uncompetitive inhibition of IMPDH. To assess the inhibition of IMPDH by the theophylline-MPA derivative, we measured the IC_{50} and

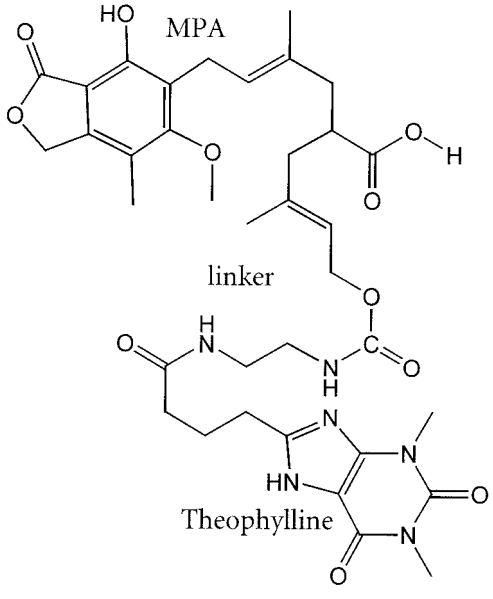

Fig. 1. Theophylline derivative of mycophenolic acid (MPA-5′-isoprenyltheophylline).

compared it with the IC_{50} for MPA *(3)*. Both compounds were diluted to eight different concentrations in 750 mL/L dimethyl sulfoxide (DMSO)–250 mL/L H_2O (75% DMSO in H_2O). IMPDH-II was diluted to 3 U/L in 100 mmol/L Tris-HCl, 100 mmol/L KCl, 3 mmol/L EDTA, 100 mg/L bovine serum albumin, 5 mmol/L tris(2-carboxyethyl)phosphine-HCl, pH 8.0. The reaction buffer was 125 mmol/L Tris-HCl, 125 mmol/L KCl, 3.75 mmol/L EDTA, 125 mg/L bovine serum albumin, 0.0625 mmol/L IMP, 0.125 mmol/L NAD, pH 8.0. The theophylline-MPA derivative was synthesized by Roche Diagnostics Corp. Human IMPDH-II was used in all assays and was produced by recombinant techniques. The enzyme was partially purified by ammonium sulfate precipitation. The IC_{50} assay was performed on the Roche COBAS FARA II analyzer. The assay reaction temperature was 40 °C. Before the assay, 40 μL of sample (DMSO-H_2O blank or eight concentrations of test compound) and 320 μL of reaction buffer were pipetted together and incubated for 5 min to warm to reaction temperature. The reaction was started by pipetting 40 μL of enzyme reagent into the cuvette. The absorbance at 340 nm was read every 30 s for 10.5 min.

Results were calculated as ΔA_{340}/min with a read window of 0.5–10.5 min. Each concentration of MPA and theophylline-MPA was run three times in triplicate (total of nine tests). In each analytical run, triplicate values were averaged and entered into Sigma Plot Ver. 4.01, which was then used to calculate the IC_{50} by a hyperbolic decay two-parameter regression: $y = ab/(b + x)$. The average IC_{50} (three analytical runs) for each compound was reported. The results were as follows: MPA, IC_{50} = 34 nmol/L (CV = 6.0%; R^2 = 0.995); MPA-5′-isoprenyl-theophylline (racemic), IC_{50} = 116 nmol/L (CV = 1.8%; R^2 = 0.984). Thus, the theophylline-MPA derivative inhibited IMPDH activity but was less inhibitory than MPA itself.

Immunoassays for theophylline were performed on the Hitachi 917 analyzer as follows: 3 μL of sample was added to a cuvette, and 150 μL of R1 reagent was added, mixed, and incubated at 37 °C for 5 min. R2 reagent (150 μL) was then added and mixed. The change in absorbance at 340 nm was monitored during the 3.5–5.0-min interval after the addition of the R2 reagent. In-house theophylline calibrators were used with the Hitachi 917 analyzer for the theophylline-MPA method. Roche Integra theophylline calibrators and a Roche Integra fluorescence polarization theophylline reagent cassette were used with the Roche Integra 700 analyzer for the method-comparison studies.

The R1 reagent formulation used was 100 mmol/L Tris, 100 mmol/L KCl, 80 mmol/L IMP, 4 mmol/L TCEP, 6 mmol/L EDTA, 1.47 μmol/L theophylline-MPA, 4 mmol/L Suttocide A, 0.1 g/L (theophylline) monoclonal antibody, IMPDH-II (adjusted to rate), final pH 8.0. The R2 reagent formulation used was 1 mmol/L NAD, 4 mmol/L Suttocide A, 1.75 mL/L Nonidet P-40 (0.175%), final pH 6.0. The (theophylline) monoclonal antibody was a purified Roche Diagnostics monoclonal.

The principle of the assay is as follows: Theophylline-specific antibody binds theophylline-MPA in the absence of theophylline and thus prevents the inhibition of IMPDH by theophylline-MPA. The enzyme activity is greatest when theophylline is absent. Theophylline, when present, binds to its antibody, thus freeing up theophylline-MPA. Free theophylline-MPA binds to catalytically active IMPDH and inhibits the enzyme by preventing the release of XMP. The rate of formation of NADH is measured at 340 nm and is correlated to theophylline concentration. The rates observed with 0, 5, 10, 20, and 40 mg/L theophylline calibrators were, respectively: 105, 98, 93, 85, and 78 milliabsorbance units/min at 340 nm on the Hitachi 917 analyzer.

We used Passing–Bablok regression statistics to compare the theophylline-MPA method on the Hitachi 917 with the fluorescence polarization method on the Integra 700. Patient plasma samples were used in the method comparison. Regression statistics were as follows: $y = 0.962x + 0.077$; median distance (95) = 1.991; n = 51; R = 0.982; median, 11.3 (x), 10.8 (y); minimum, 8.3 (x), 8.8 (y); maximum, 29.5 (x), 31.0 (y).

We conclude that these results indicate the potential use of IMPDH as a homogeneous enzyme immunoassay technology as shown for theophylline.

References

1. Fleming MA, Chambers SP, Connelly PR, Nimmersgern E, Fox T, Bruzzese FJ, et al. Inhibition of IMPDH by mycophenolic acid: dissection of forward and reverse pathways using capillary electrophoresis. Biochemistry 1996;22: 6990–7.
2. Carr SF, Papp E, Wu JC, Natsumeda Y. Characterization of human type I and type II IMP dehydrogenases. J Biol Chem 1993;36:27286–90.
3. Nelson PH, Carr SF, Devens BH, Eugui EM, Franco F, Gonzalez C, et al. Structure-activity relationships for inhibition of inosine monophosphate dehydrogenase by nuclear variants of mycophenolic acid. J Med Chem 1996;21:4181–96.

Active Electronic Arrays for Genotyping of *NAT2* Polymorphisms, *Youvraj R. Sohni,[1] Brian Dukek,[1] William Taylor,[2] Elena Ricart,[3] William J. Sandborn,[3] and Dennis J. O'Kane[1,2*]* ([1] Department of Laboratory Medicine and Pathology, [2] Mayo Clinic Cancer Center, and [3] Division of Gastroenterology and Hepatology, Mayo Clinic, Rochester, MN 55905; * address correspondence to this author at: Hilton 730, Department of Laboratory Medicine and Pathology, Mayo Clinic, Rochester, MN 55905; fax 507-284-9758, e-mail okane.dennis@mayo.edu)

The *N*-acetyltransferase 2 (*NAT2)* gene is autosomal, dominant, and intronless with an open reading frame of 870 bp. It is located on chromosome 8p22. NAT2 enzyme detoxifies and inactivates drugs and xenobiotics in the liver. *NAT2* polymorphisms confer phenotypes categorized as slow, intermediate, or rapid acetylators with broad interethnic variation. There are 26 known alleles, and each allelic variant is a combination of one, two, three, or four nucleotide substitutions. Within the coding

region there are seven missense mutations (G191A, T341C, A434C, G590A, A803G, A845C, and G857A) and four silent mutations (T111C, C282T, C481T, and C759T) *(1, 2)*. The wild-type *NAT2*4* allele is associated with the rapid acetylator phenotype and does not have any nucleotide substitutions. The phenotype can be predicted with 95% accuracy by genotyping. *(3–5)*.

We present a method for performing multiple-polymorphism genotyping of the *NAT2* gene. A single amplification of *NAT2* is performed with sequential probing for multiple polymorphisms by active electronic arrays. The method permits application of multiple DNA samples in singleton for high-throughput genotyping. Rapid high-throughput determination of genotypes may aid in clinical epidemiology studies and in routine clinical practice.

Published primer sequences were used to perform PCR to generate a 1212-bp amplicon *(6)*. The primers were 5′-AAT TAG TCA CAC GAG GA-3′ (forward) and 5′-biotin-TCT AGC ATG AAT CAC TCT G-3′ (reverse). The biotinylated primers permit capturing of the amplicons to the microarray surface where they remain embedded through interaction with streptavidin in the permeation layer. The agarose permeation layer containing streptavidin coats the microarray, separating the biological materials from the harsh electrochemical environment, and allows binding of biotinylated amplicons *(7)*.

The PCR reaction mixture consisted of 5 μL of 10× buffer (Applied Biosystems), 1 μL of dNTPs (10 mM each dNTP; Roche), 5 μL (50 μM) of each primer, 0.25 U of AmpliTaq Gold, and 200–400 ng of DNA template. The thermal cycling conditions were as follows: 95 °C for 10 min; 30 cycles of 94 °C for 1 min, 55 °C for 1 min, and 72 °C for 2 min; and final extension at 72 °C for 5 min. At the end of PCR, the products were desalted on MultiScreen® PCR plates (Millipore) and resuspended in water.

We prepared hybridization mixtures to address the amplicons to Nanochip™ array sites (Nanogen). A hybridization mixture consisted of 5–40 nmol/L desalted amplicons, 250 nmol/L each stabilizer oligonucleotide, and 40 μL of 100 mmol/L L-histidine buffer in a total volume of 80 μL. The following stabilizer oligonucleotides were used: 5′-TGA CAG GAA TTA CAT TGT CGA TGC-3′ (*NAT2**T341C), 5′-AAA TAT ATT TAA GAT TTC CTT GGG GAG AAA TCT CGT G-3′ (*NAT2**A803G), and 5′-GGG TGG GTG GTG TCT CCA GGT CAA T-3′ (*NAT2**G191A). The hybridization mixtures were denatured at 95 °C for 10 min before they were transferred to a Nunc V-bottomed plate for loading. The Nunc plates containing the hybridization mixtures were loaded in the instrument loader. A mapping protocol was used to electronically address biotinylated amplicons to user-designated sites on the microarray. Instrument software was used to create a map to address the hybridization mixtures to designated sites on the chip array. A negative control oligonucleotide (ATA5) and a L-histidine buffer blank were addressed to the array simultaneously with the test amplicons.

Temperature was used to discriminate between matched and mismatched reporters. The reporters had the single-nucleotide polymorphism (SNP) as the 3′ terminal base and a fluorophore at the 5′ end. The wild-type reporter probe was labeled with Cy5 and the polymorphism probe with Cy3 in all cases. The following reporter probes were synthesized: 5′-CAG GTG ACC AT/C-3′ (T341C), 5′-GAA GTG CTG AA/G-3′ (A803G), and 5′-AAG AAG AAA CCG-3′ and 5′-TAA GAA GAA ACC A-3′ (G191A; Integrated DNA Technologies). The SNP reporting mixture consisted of 500 nmol/L each reporter and 48 μL of high-salt buffer in a final volume of 50 μL. The microarray was imaged using separate lasers for both Cy5 and Cy3. The optimal temperature was determined for each locus by a temperature-ramping fluorescence reader protocol. A user-designated protocol was designed by which the array was subjected to 2 °C increments in temperature followed by scans at ambient temperature after each ramp. Initially, the array was scanned over a wide range of temperatures. The optimal temperature was selected for scanning the array for fluorescence intensity.

Known heterozygotes were used to normalize hybridization efficiency between Cy5 and Cy3 dye-labeled reporters. Heterozygotes were verified by dye-terminator sequencing on ABI 377 DNA sequencers in both forward and reverse directions. A biallelic fluorescence intensity ratio ≤1:3 was defined as heterozygous and a ratio ≥1:5 was defined as homozygous. Genotypes were assigned using the manufacturer's recommended biallelic fluorescence intensity ratios. No genotype designations were made for fluorescence intensity ratios between 1:3 and 1:5. Homozygous wild-type alleles hybridized with Cy5-labeled reporter probe, whereas homozygous polymorphic alleles hybridized only with Cy3-labeled reporter probes. Each heterozygous complex hybridized with both labeled probes for each allele pair tested.

Sequential probing with reporter probe pairs was used to analyze each SNP in the amplicon. The A803G polymorphism was detected first because of the relatively lower T_m for its reporters. At the end of the first reporting, the array was subjected to a reporter dehybridization protocol in the fluorescence reader. Using this protocol, we stripped the probes from the array by ramping the temperature to 40 °C followed by a L-histidine buffer wash. We confirmed complete probe dehybridization by verifying the absence of any fluorescence signal. We then sequentially reprobed with the reporters for G191A followed by T341C.

Representative genotyping results for the *NAT2**T341C polymorphism are shown in Fig. 1. The genotype designation for amplicon 1 is homozygous for the polymorphic allele. This is based on a fluorescence intensity ratio ≥1:5 between Cy3 and Cy5 dye-labeled reporters. Furthermore, the data are normalized with a known heterozygote confirmed previously by sequencing. Similarly, the genotype designation for amplicon 10 is homozygous for the wild-type allele. The genotypes for the remaining sample amplicons shown in Fig. 1 are designated as heterozygous with Cy5/Cy3 biallelic fluorescence ratios ≤1:3.

Overall, for *NAT2**T341C, 79 of 83 (95.2%) amplicons

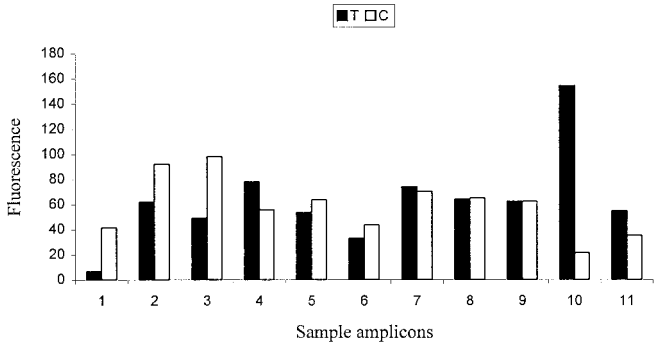

Fig. 1. Representative genotyping results for the *NAT2**T341C polymorphism.

were genotyped in a single hybridization run on one microarray. Of these, 32.5% were wild type, 50.6% were heterozygous, and 12% were homozygous for the polymorphism (Table 1). For *NAT2**A803G, 80 of 83 (96.4%) amplicons were genotyped in a single hybridization run on a microarray, of which 34.9% were wild type, 49.4% were heterozygous, and 12% were homozygous for the polymorphism. For *NAT2**G191A, 71 of 83 (86%) amplicons were genotyped in a single run, of which 100% were wild type.

In practice, <100% of samples could be genotyped in a single run. For *NAT2**T341C, there were three amplicons that could not be assigned a genotype because the biallelic ratio was between 1:3 and 1:5. There were two amplicons for *NAT2**A803G and six amplicons for *NAT2**G191A that were not assigned a genotype for the same reason. Of the 83 amplicons that were analyzed, there was only one DNA sample that could not be genotyped for any of the SNPs because of failed PCR. This may be attributable to the poor quality of the template DNA used for PCR or to human error in either the PCR set-up or genotyping steps. In some cases, in spite of successful PCR, the amplicon(s) had a lower DNA concentration than required. There were five *NAT2**G191A amplicons for which the fluorescence signals were too low to make a designation. Furthermore, three sets of stabilizers and reporters were used for the three different SNPs that were analyzed. Although sequential probing was done on the same amplicon, the amplicon concentration thresholds required for the three SNPs were different. This is because of differences in base-pairing interactions among the stabilizers and target DNA as well as differences in base-stacking interactions between stabilizer and reporter pairs. It is therefore possible that, whereas one SNP could be assayed successfully for a test amplicon, analysis of another SNP on the same amplicon failed.

Microarray genotyping results were confirmed by direct DNA sequencing with 100% concordance. Sequential scanning for polymorphisms within an amplicon could be performed up to five times without significant degradation of the signal-to-noise ratio. This approach has been extended to four additional four SNPs (C282T, C481T, G590A, and G857A), using a second microarray, and achieved comparable results.

Sequential probing is a rapid and accurate method for genotyping multiple polymorphisms in large amplicons and intronless genes. The method can be applied to test large number of samples, using active electronic arrays. This sequential probing approach is particularly useful in epidemiologic studies because of its relative simplicity and high sample throughput, which could improve the cost-effectiveness for genotyping.

Table 1. Genotyping results for *NAT2* polymorphisms in this study.

SNP	Genotyped/single run	Wild type[a]	Heterozygous	Mutant[a]
T341C (n = 83)	79/83 (95.2%)	32.5%	50.6%	12%
A803G (n = 83)	80/83 (96.4%)	34.9%	49.4%	12%
G191A (n = 83)	71/83 (86%)	100%	0	0

[a] Homozygous.

References

1. Grant DM, Hughes NC, Janezic SA, Goodfellow GH, Chen HJ, Gaedigk A, et al. Human acetyltransferase polymorphisms. Mutat Res 1997;376:61–70.
2. Hein DW, Doll MA, Fretland AJ, Leff MA, Webb SJ, Xiao GH, et al. Molecular genetics and epidemiology of the *NAT1* and *NAT2* acetylation polymorphisms. Cancer Epidemiol Biomark Prev 2000;9:29–42.
3. Hickman D, Sim E. *N*-Acetyltransferase polymorphism: comparison of phenotype and genotype in humans. Biochem Pharmacol 1991;42:1007–14.
4. Grant DM. Molecular genetics of the *N*-acetyltransferases. Pharmacogenetics 1993;3:45–50.
5. Cascorbi I, Drakoulis N, Brockmoller J, Mauer A, Sperling K, Roots I. Arylamine *N*-acetyltransferase (*NAT2*) mutations and their allelic linkage in unrelated Caucasian individuals: correlation with phenotypic activity. Am J Hum Genet 1995;57:581–92.
6. Agundez JAG, Martinez C, Olivera M, Ledesma MC, Ladero JM, Benitez J. Molecular analysis of the arylamine *N*-acetyltransferase polymorphism in a Spanish population. Clin Pharmacol Ther 1994;56:202–9.
7. Gilles PN, Wu DJ, Foster CB, Dillon PJ, Chanock SJ. Single nucleotide polymorphic discrimination by an electronic dot blot assay on semiconductor microchips. Nature Biotechnol 1999;17:365–70.

Mass Spectroscopy as a Discovery Tool for Identifying Serum Markers for Prostate Cancer, *John J. Hlavaty,[1] Alan W. Partin,[2] Felicity Kusinitz,[1] Matthew J. Shue,[2] Adam Stieg,[1] Kate Bennett,[1] and Joseph V. Briggman[1*]* ([1] Matritech, Inc., 330 Nevada St., Newton, MA 02460; [2] The James Buchanan Brady Urological Institute, The Johns Hopkins Hospital, Baltimore, MD 21287-0033; * author for correspondence: fax 617-928-0821, e-mail jhlavaty@matritech.com)

Prostate cancer is the second most common malignancy in men, after skin cancer, and the second most common cause of cancer death in men over age 60 years, after lung cancer. This year, ~198 100 new cases of prostate cancer will be diagnosed in the US, and an estimated 31 500 men will die of prostate cancer *(1)*. Five-year survival is close to 100% when the disease is diagnosed and treated with definitive local therapy while it is still organ-confined, but in approximately one-third of men diagnosed with clinically localized disease, the disease has spread beyond the confines of the prostate at the time of surgery *(2, 3)*.

The Food and Drug Administration approved a serum

test for prostate-specific antigen (PSA) in the 1980s. With an upper reference limit in serum of 4 μg/L, 67–80% of prostate cancers can be detected, for a positive predictive value of 24% *(4, 5)*. Combining the serum PSA test with a digital rectal examination can improve the positive predictive value *(3, 6, 7)*. Despite the availability of the PSA test and the moderately high compliance with routine testing recommendations, ~20–30% of prostate cancers are missed by the current early detection protocols. The identification of more accurate serum markers for prostate cancer could improve the current clinical capabilities for cancer detection and may reduce cancer mortality.

Proteomics, the large-scale comparison of protein expression patterns, can be used to identify proteins that are associated with disease states such as cancer. These studies have been enhanced by the development of powerful and sensitive new methods, such as matrix-assisted laser desorption/ionization time-of-flight mass spectrometry (MALDI-TOF). In this technique, proteins are adsorbed to a solid matrix, desorbed with a pulsed laser beam to produce gas-phase ions that traverse a field-free flight tube, and then separated according to their velocities, which depend on their mass/charge ratio. The sensitivity of this method for protein identification has been improved by the development of surface-enhanced laser desorption/ionization time-of-flight mass spectrometry (SELDI-MS). SELDI is an affinity-based MS method in which proteins are selectively adsorbed to a chemically modified surface, impurities are removed by washing with buffer, an energy-absorbing material is layered on top, and the proteins are identified by laser desorption mass analysis. SELDI protein analysis has been used to detect prostate cancer-associated proteins in cancer cell lysates, seminal plasma, and serum *(8, 9)*. We report here the use of SELDI to identify a putative prostate cancer-specific protein in the preoperative serum of patients with histologically confirmed prostate cancer.

Serum samples were obtained from The Johns Hopkins School of Medicine (Baltimore, MD). For men with prostate cancer, serum samples were obtained before surgery. Serum samples also were obtained from age-matched controls clinically determined to be cancer-free (serum PSA concentration <2 μg/L and an unremarkable digital rectal exam). All samples were collected with informed consent according to protocols approved by the Institutional Review Board. Serum samples were stored at −80 °C before analysis.

The serum samples were partially purified to remove interfering serum components, fractionated by ion-exchange chromatography, and analyzed by SELDI in a process known as "retentate mapping". Briefly, sera were treated with 1,1,2-trichloro-trifluoroethane to remove lipids, passed over a HiTrap Protein G column (Pharmacia Biotech) to remove immunoglobulins, and then passed over a HiTrap Blue column (Pharmacia Biotech) to remove human serum albumin. The samples were fractionated over a Protein-Pak Q 8HR column (Waters) with a 14-step NaCl step gradient in the concentration range of 0–1 mol/L. Throughout sample preparation, 50 mmol/L NaH_2PO_4, pH 7.0, was used as the buffer.

Cancer-specific serum protein markers were identified by a three-stage screening strategy. In the first stage, a set of putative prostate cancer biomarkers was identified by comparing sera from five patients whose prostate cancer showed capsular penetration with sera from five cancer-free controls. Each of the 14 fractions from each sample was applied to four different ProteinChips™ (Ciphergen Biosystems): H4, which has a hydrophobic surface for reversed-phase binding; WCX-2, which binds cationic proteins; IMAC-3-Ni^{2+}, which binds proteins with an affinity for nickel; and SAX-2, which binds anionic proteins. Samples were analyzed in a Ciphergen Series PBS-I ProteinChip System (SELDI mass spectrometer). Ciphergen system software was used to produce composite spectra for each fraction assayed on each chip from the prostate cancer and control samples. The software generated difference spectra that identified four novel peaks (59.7, 22.7, 21.4, and 50.8 kDa) that were present in the cancer samples but not in the controls. These peaks were identified with the H4, WCX-2, and IMAC-3 ProteinChips. A novel peak was defined as having an amplitude at least threefold greater than the baseline.

In the second stage of biomarker identification, an additional 15 cancer serum samples and 15 healthy serum controls were analyzed under the specific conditions used to identify the four putative markers, i.e., each marker was analyzed from a single ion-exchange fraction with a single ProteinChip. On the basis of combined analysis of all of the samples, one novel protein peak was found in all 20 cancer samples but not in any of the prostate cancer-free controls. This was a 50.8-kDa protein identified in the 125 mmol/L salt fraction with the WCX-2 ProteinChip. Representative SELDI profiles are illustrated in Fig. 1.

In the third stage of biomarker identification, 16 additional prostate cancer serum samples were assayed for the presence of the 50.8-kDa peak. The 50.8-kDa protein peak was found in all 36 cancer serum samples (5 from the first stage, 15 from the second stage, and 16 from the third stage of biomarker identification). Studies are now underway to purify and identify the 50.8-kDa polypeptide. This will allow us to elucidate its biochemical association with prostate cancer and develop a sensitive and specific assay that is suitable for prostate cancer screening.

All of the controls and all but two of the cancer patients had serum PSA concentrations tested. Eight of the 34 prostate cancer patients who were tested (24%) had preoperative serum PSA concentrations <4 μg/L, the recommended age-adjusted cutoff for men at least 50 years of age who are otherwise healthy, nonsymptomatic, and have no prior risk for prostate cancer. One of these cancers was organ-confined, and the other seven demonstrated capsular penetration on histologic examination of the resected prostate. All eight of these cancer patients were missed by PSA serum testing but were identified by SELDI analysis of the 50.8-kDa serum protein.

Four of the 18 patients (22%) with PSA between 4.1 and 10 μg/L had tumors with capsular penetration, whereas all 5

patients with PSA between 10.1 and 20 μg/L and all 3 patients with PSA >20 μg/L had tumors with capsular penetration. The probability of organ confinement decreases with increasing preoperative serum PSA concentrations, although PSA testing alone is not completely predictive *(2)*. SELDI analysis conducted in the way we describe is only qualitative, so no direct correlation of concentration could be made with either PSA concentration or tumor grade.

PSA is synthesized predominately in the epithelium of the prostate gland and the periurethral glands; therefore, serum PSA should disappear after radical prostatectomy because the tissue source is removed. Serum PSA concentration is used as a surrogate endpoint for postoperative disease management: the failure of serum PSA to disappear after surgery indicates the presence of persistent disease, and the recurrence of serum PSA signals either cancer recurrence or metastasis. Patients with metastatic prostate cancer typically undergo androgen ablation therapy, which can be effective in suppressing recurrence and metastasis. However, because PSA synthesis and secretion require hormonal influence, androgen suppression can reduce PSA production *(4)*. Therefore, even if occult metastatic sites should develop, they might not secrete enough PSA into the serum to exceed the diagnostic threshold set for routine screening. Another serum marker, preferably androgen-independent, would be a great asset for monitoring prostate disease after surgery.

All of the serum samples tested in this study were collected preoperatively. The findings in this work are promising, but preliminary. It would be informative to test postoperative serum samples for the disappearance of the 50.8-kDa protein and to compare this with serum PSA and clinical disease progression.

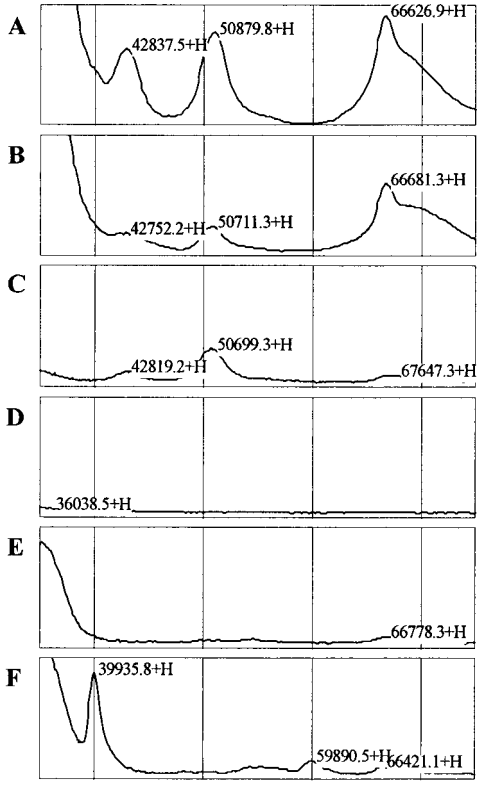

Fig. 1. Representative SELDI protein profiles from fractionated serum samples from three prostate cancer patients (*A–C*) and three controls (*D–F*).

Samples collected in 125 mmol/L NaCl from a Protein-Pak Mono-Q ion-exchange column were applied to WCX-2 ProteinChips and analyzed in a Ciphergen PBS-1 ProteinChip reader. A single protein peak appearing at 50.8 kDa was found in all 36 prostate cancer samples but in none of the 20 clinically determined prostate cancer-free controls. A novel peak was defined as having an amplitude at least threefold greater than the baseline.

We acknowledge Natalie S. Rudolph for help in preparing the manuscript.

References

1. Greenlee R, Hill-Harmon MB, Murray T, Thun M. Cancer statistics, 2001. CA Cancer J Clin 2001;51:15–36.
2. Partin A, Kattan MW, Subong ENP, Walsh PC, Wojno KJ, Oesterling JE, et al. Combination of prostate-specific antigen, clinical stage and Gleason score to predict pathological stage of localized prostate cancer. JAMA 1997;277: 1445–51.
3. Smith R, von Eschenbach AC, Wender R, Levin B, Rothenberger D, Brooks D, et al. American Cancer Society Guidelines for the early detection of cancer: update of early detection guidelines for prostate, colorectal, and endometrial cancers and update 2001: testing for early lung cancer detection. CA Cancer J Clin 2001;51:38–75.
4. Polascik TJ, Oesterling JE, Partin AW. Prostate specific antigen: a decade of discovery—what we have learned and where we are going. J Urol 1999;162: 293–306.
5. Carroll P, Coley C, McLeod D, Schellhammer P, Sweat G, Wasson J, et al. Prostate-specific antigen best practice policy. Part I. Early detection and diagnosis of prostate cancer. Urology 2001;57:217–24.
6. Catalona W, Richie J, Ahmann F, Hudson M, Scardino P, Flanigan R, et al. Comparison of digital rectal examination and serum prostate specific antigen in the early detection of prostate cancer: results of a multicenter clinical trial of 6,630 men. J Urol 1994;151:1283–90.
7. National Cancer Institute. CancerNet PDQ cancer information summaries. Screening for prostate cancer. http://www.cancernet.nci.nih.gov/pdq.html (accessed May 19, 2001).
8. Paweletz C, Gillespie J, Ornstein D, Simone, NL, Brown MR, Cole KA, et al. Rapid protein display profiling of cancer progression directly from human tissue using a protein biochip. Drug Dev Res 2000;49:34–42.
9. Wright G, Cazares L, Leung S, Nasim S, Adam B, Yip T, et al. ProteinChip surface enhanced laser desorption/ionization (SELDI) mass spectrometry: a novel protein biochip technology for detection of prostate cancer biomarker in complex protein mixtures. Prostate Cancer Prostate Dis 1999;2:264–76.

Allergen-specific IgE Detection on Microarrays Using Rolling Circle Amplification: Correlation with in Vitro Assays for Serum IgE, *Michael C. Mullenix,[1*] Steve Wiltshire,[1] Weiping Shao,[1] Gary Kitos,[2] and Barry Schweitzer[1]* ([1] Molecular Staging Inc., 300 George St., Suite 701, New Haven, CT 06511; [2] Esoterix Inc., 201 Summit View Dr., Suite 100, Brentwood, TN 37027; * author for correspondence: fax 203-772-5276, e-mail mikem@molecularstaging.com)

Allergen-specific IgE antibody in patient serum is used to predict an allergic response in individuals with concordant clinical history. For more than 30 years, in vitro assays for allergen-specific IgE have been used along with or in place of skin-prick allergen testing (SPT) *(1)*. In vitro test methods include various immunoassay formats with

solid-phase supports such as paper disks, microtiter plates, nitrocellulose, and microparticles. The field has advanced with immunoassay refinements, including solid phases with higher allergen-binding capacities, monoclonal antibodies for detection, enzyme amplification systems, and fluid-phase allergen/IgE complex formation; these have improved the sensitivity of the in vitro assays and provided better correlation to skin-prick allergen tests *(2–4)*.

SPT and in vitro allergen-specific IgE assays have advantages and disadvantages. SPT results are available immediately, allowing the allergist to provide treatment while the patient is still in the office. Multiple allergen extracts are tested simultaneously on the same patient. Skin-prick tests have the highest positive predictive value because they are biological, but they also have a high false-positive rate. To be administered in vivo, the allergen extracts must be sterile and of low toxicity to prevent anaphylaxis. SPT is expensive because it requires a skilled practitioner. In vitro serum allergen-specific IgE immunoassays are semiquantitative and allow testing of an allergic response over time *(4)*. They are minimally invasive, with no risk of an adverse reaction in the patient, and are the best option in patients with severe skin conditions such as eczema, urticaria, or dermatographism. In food allergy testing, in vitro tests can reduce by one-half the need for oral allergen challenges *(4)*. In vitro tests can also be used with patients receiving medications, such as antihistamines, that may interfere with SPT responsiveness. However, results of in vitro IgE assays can vary between test formats as well as between laboratories performing the same assay *(5)*.

An adaptation of rolling circle amplification (RCA) *(6)*, termed "immunoRCA", for very sensitive detection and measurement of proteins has been described recently *(7)*. In immunoRCA, the 5′ end of an oligonucleotide primer is attached to an antibody; thus, in the presence of circular DNA, DNA polymerase, and nucleotides, the rolling circle reaction produces a concatamer of circle DNA sequence copies that remain attached to the antibody. The amplified DNA is detected by hybridization of fluorescently labeled, complementary oligonucleotide probes. When performed on a solid phase, immunoRCA allows substantial multiplexing because signal amplification occurs on the immobilized detection antibody rather than in solution. ImmunoRCA is thus well suited as an amplification technique in microarray immunoassays *(7)*.

We previously demonstrated that detecting allergen-specific IgE on microarrays using immunoRCA provided results that were in excellent agreement those obtained with SPT *(8)*. In the present study, we compare results obtained by immunoRCA on microarrays with those obtained from two commercially available allergen-specific IgE assays and one in-house reference laboratory test. Forty-four serum samples were selected to provide 6 positive and 5 negative serum samples for each of the following four allergens: cat dander, dust mites (*Dermatophagoides farinae*), short ragweed, and peanuts. The positive serum samples were prepared by pooling three to five patient sera to provide one positive serum sample for each of the six concentrations used in the alternative scoring method (ASM) for allergen-specific IgE assays. We used the Pharmacia CAP system to assign ASM scores to patients' sera. Each negative serum sample corresponded to a single patient. All characterized serum samples were analyzed simultaneously in the Pharmacia CAP system, the DPC AlaSTAT system, and the Esoterix Allergy and Asthma system immunoassays to measure correlation to the described microarray assay. Commercial assay testing was carried out at Esoterix Allergy and Asthma (Gainesville, FL).

ImmunoRCA assays on allergen microarrays were carried out on all 44 samples as described previously with minor modifications *(8)*. Microarrays of cat dander, dust mite, short ragweed, and peanut extracts were blocked with 2 g/L bovine serum albumin in 50 mmol/L glycine (pH 9.0) for 1 h at 37 °C. After incubation, the slides containing the microarrays were washed twice in phosphate-buffered saline (PBS) containing 0.5 mL/L Tween 20 by soaking for 2 min in Coplin jars. Patient serum (10 μL) was added to individual microarrays and incubated for 30 min at 37 °C. The microarrays were washed twice in PBS containing 0.5 mL/L Tween 20. Biotinylated polyclonal goat anti-human IgE (20 μL of a 5 mg/L solution; BiosPacific) was added to each microarray and incubated for 30 min at 37 °C; the microarrays were then washed twice. An anti-biotin monoclonal antibody (Jackson ImmunoResearch) conjugated to a 35mer oligonucleotide RCA primer, as described previously *(7)*, was mixed with 200 nmol/L complimentary single-stranded circular DNA in PBS containing 0.5 mL/L Tween 20 and 1 mmol/L EDTA and incubated at 37 °C for 30 min. Conjugate preannealed to circular DNA (20 μL of a 5 mg/L solution) was added to each array and incubated at 37 °C for 30 min. After conjugate binding, the microarrays were washed with PBS containing 0.5 mL/L Tween 20. The RCA reaction was carried out at 37 °C for 30 min with T7 native polymerase, and the product of the RCA reaction was detected by fluorescently labeled probes as described previously *(7)*. Slides were scanned on a GSI Lumonics ScanArray 5000 microarray scanner, and the fluorescence was quantified by QuantArray software.

All serum samples that were positive by the Pharmacia CAP assay for a particular allergen demonstrated a dose-dependent ASM score when IgE concentrations for that allergen were measured by immunoRCA (Fig. 1). Furthermore, none of the serum samples negative for a particular allergen in the Pharmacia CAP assay produced a fluorescence intensity in the immunoRCA assay that was greater than the corresponding lowest ASM score sample for that allergen. None of the 44 samples tested gave false-negative or -positive test results. Although the positive serum samples were prepared from pools of sera from three to five patients and may not fully represent an unselected population, the results indicate that the immunoRCA microarray assay correlates with ASM scores assigned using the Pharmacia CAP assay.

To determine the correlation of the immunoRCA mi-

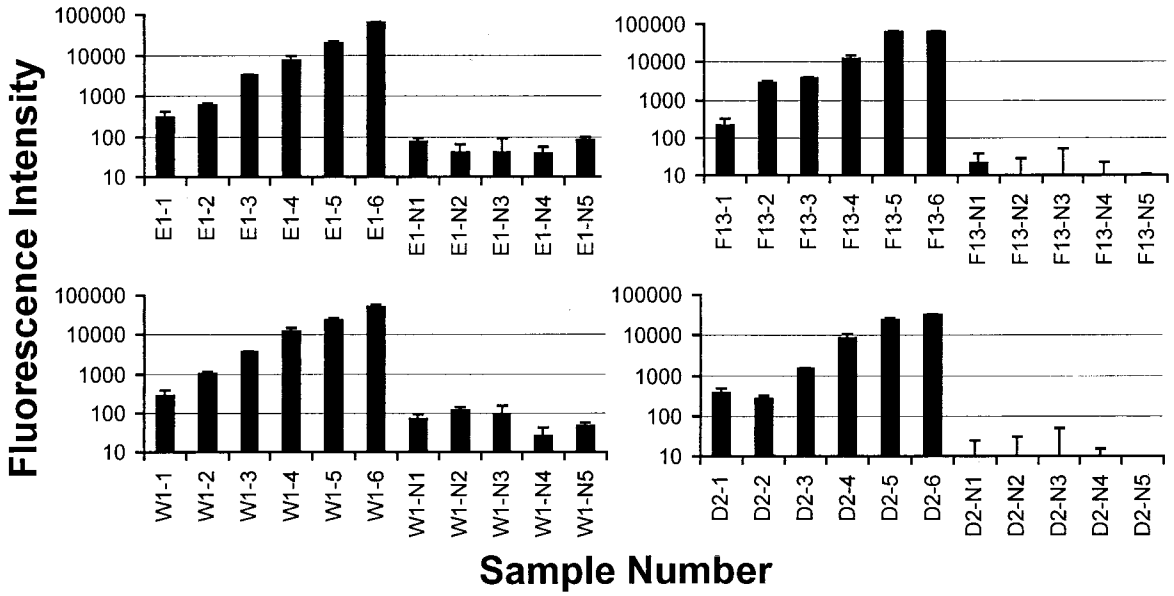

Fig. 1. ImmunoRCA allergen-specific IgE detection on microarrays.

Six positive and five negative serum samples for each of four allergens were tested in the immunoRCA microarray allergen-specific IgE assay. Samples are designated *E1* for cat dander, *F13* for peanut, *W1* for short ragweed, and *D2* for dust mite (*D. farinae*). Negative samples are identified with an *N* after the hyphen. In positive samples, the *number* after the hyphen indicates the ASM score.

croarray assay with other commercial assays, the positive and negative serum samples were tested simultaneously in three commercial allergen-specific IgE assays, and correlation coefficients were calculated based on all 44 samples (Table 1). All of the comparisons produced correlation coefficients >0.9, indicating a high correlation between the immunoRCA microarray assay and the other commercial methods. The results indicate that the specificity and sensitivity of the immunoRCA microarray immunoassay for allergen-specific IgEs are comparable to those for commercial assays.

To demonstrate the lower limit of detection and dynamic range of the immunoRCA assay, the peanut-positive serum with an ASM score of 6 was serially diluted in negative serum and tested on microarrays and in the three commercial assays (data not shown). The immunoRCA assay was linear over a 4456-fold dilution range, and the lower limit of detection was at least 10-fold lower than the detection limits for the commercial assays.

An important advantage of microarray assays is the ability to multiplex. The immunoRCA microarray assay is capable of simultaneously screening hundreds of allergens. Microarrays also include internal control spots and calibrators, allowing more rigorous standardization of the results than is possible in other formats. Microarray assays require <1 nL of allergen extract per test, which allows the use of the more expensive allergen extracts used for SPT in microarray production. Use of the SPT extracts may be a factor behind the superior clinical accuracy reported for the microarray allergen-specific IgE assay *(8)* compared with the CAP assay, which uses crude allergen extracts. Another advantage of microarray assays, which may be of particular value in pediatric patients, is the requirement for only 10 μL of serum in these assays. The 10-μL serum volume may allow the use of finger pricks in place of venipuncture for collection of test samples.

Table 1. Correlation[a] between microarray assay and commercial clinical allergen-specific IgE assays.

	Correlation coefficient		
Allergen	**DPC AlaSTAT**	**Esoterix Modified RAST**	**Pharmacia CAP**
Peanut	0.900	0.900	0.984
Cat dander	0.982	0.906	0.971
Short ragweed	0.954	0.992	0.986
Mite (*D. farinae*)	0.975	0.996	0.999

[a] Correlation coefficients were calculated to compare two data sets with different units of measurement *(9)*.

ImmunoRCA allergen-specific IgE microarray assays can provide a powerful screening tool for allergists. Microarray assays for use in an allergy clinic can be separated into panels of allergens to be tested concurrently. The panels can cover allergens falling into similar categories, such as inhaled allergens, food allergens, or drug allergens. Arrays corresponding to these panels can be customized to reflect regional differences in environmental allergens. The immunoRCA microarray assay uses a 16-well format in which the arrays are separated by a Teflon mask. The wells can hold 100–400 spots, thus allowing thousands of assays to be completed per slide. Additionally, the microarray layout allows the assay to be automated using a Beckman BioMek liquid-handling robot.

ImmunoRCA microarray assays are capable of providing quantitative results *(7)*. Quantitative allergen-specific

IgE assays allow allergists to accurately monitor immunotherapy techniques, screen infants and small children for atopic allergen sensitivities, limit the need for oral challenges with food allergens, and monitor the effectiveness of allergen avoidance strategies *(4)*. Quantitative microarray assays are calibrated with calibration curves generated from serial dilutions of target analytes or dilutions of target analytes immobilized directly on the surface of each microarray. The advantage to the second approach is that each microarray contains its own internal calibration curve, eliminating the effects of variability between arrays. We anticipate that immunoRCA microarray allergen-specific IgE assays will provide allergists with quantitative results and more information in a rapid time frame, increasing cost-effectiveness and the quality of patient care.

We would like to acknowledge Dr. R. Murli Krishna and Mehul Patel for technical assistance. We thank Drs. Stephen Kingsmore and David Edgar for expert advice and clinical insight.

References

1. Dolen WK. It is not yet time to stop skin testing, but . . . . J Allergy Clin Immunol 2000;105:1074–6.
2. Corey JP, Liudahl JJ, Young SA, Rodman SM. Diagnostic efficacy of in vitro methods vs skin testing in patients with inhalant allergies. Otolaryngol Head Neck Surg 1991;104:299–302.
3. Corey JP, Nelson RS, Lai V. Comparison of modified PhadezymeRAST, ImmunoCAP, and serial dilution titration skin testing by receiver operating curve analysis. Otolaryngol Head Neck Surg 1995;112:665–9.
4. Yunginger, JW, Ahlstedt S, Eggleston PA, Homburger HA, Nelson HS, Ownby DR, et al. Quantitative IgE antibody assays in allergic diseases. J Allergy Clin Immunol 2000;105:1077–84.
5. Szeinbach SL, Barnes JH, Sullivan TJ, Williams PB. Precision and accuracy of commercial laboratories' ability to classify positive and/or negative allergen-specific IgE results. Ann Allergy Asthma Immunol 2001;86:373–81.
6. Lizardi PM, Huang X, Zhu Z, Bray-Ward P, Thomas DC, Ward DC. Mutation detection and single-molecule counting using isothermal rolling-circle amplification. Nat Genet 1998;19:225–32.
7. Schweitzer B, Wiltshire S, Lambert J, O'Malley S, Kukanskis K, Zhu Z, et al. Immunoassays with rolling circle amplification: a versatile platform for ultrasensitive antigen detection. Proc Natl Acad Sci U S A 2000;97:10113–9.
8. Wiltshire S, O'Malley S, Lambert J, Kukanskis K, Edgar D, Kingsmore S, et al. Detection of multiple allergen-specific IgEs on microarrays by immunoassay with rolling circle amplification. Clin Chem 2000;46:1990–3.
9. Miller JC, Miller JN. Statistics for analytical chemistry, 2nd ed. Chichester: Ellis Horwood Limited, 1992:104–9.

Rapid and Automated Cartridge-based Extraction of Leukocytes from Whole Blood for Microsatellite DNA Analysis by Capillary Electrophoresis, *Phillip Belgrader, Fariba Raisi, Rekha Joshi, Peter Nguyen, William McMillan, Jesus Ching,* Ron Chang, and M. Allen Northrup* (Cepheid, 1190 Borregas Ave., Sunnyvale, CA 94089; * author for correspondence: fax 408-541-4191, e-mail ching@cepheid.com)

The human genome contains microsatellite sequences, consisting of 2- to 5-bp repeats, randomly distributed among the chromosomes. These sequences, also called short tandem repeats (STRs), have been demonstrated as important markers for disease diagnostics, genetic mapping, and human identification. The list of human hereditary diseases associated with the unusual expansion or deletion of specific microsatellite loci continues to increase. The two most understood diseases of this type are the CGG repeats in fragile-X syndrome *(1)* and the CAG repeats in Huntington disease *(2)*. However, other diseases, such as cancer of the colon, head, neck, gastrointestinal track, urinary bladder, liver, lung, breast, and leukocytes [white blood cells (WBCs)], have been shown to be linked to microsatellite instability *(3–14)*.

The growing importance of microsatellite markers in diagnostics has motivated us to develop rapid, automated devices to integrate sample preparation, PCR, and capillary electrophoresis (CE) analysis. The work presented here demonstrates an efficient filtration cartridge *(15)* to automatically process WBCs in a sample of blood for PCR amplification and CE analysis. A flow-through sample preparation procedure is used that does not require vortex-mixing, precipitation, and centrifugation, and is amenable to integration into a microfluidic circuit. *TH01*, a well-characterized microsatellite locus, served as the model for this study. *TH01*, a gene for human tyrosine hydroxylase, is a 4-bp repeat and comprises seven alleles *(16)*.

Samples of whole blood collected from seven individuals were obtained from Stanford Blood Bank (Palo Alto, CA). The blood (~10 mL) was drawn into tubes containing citrate as the anticoagulant and then stored in a refrigerator until processed on a cartridge fluidic system. For each cartridge run, sample (200 μL), isotonic solution (6.5 mL), and lysis buffer (600 μL of 10 mmol/L Tris, 150 mmol/L NaCl, 1 mL/L Triton X-100, pH 8.5) were loaded in the appropriate chambers in the cartridge (Fig. 1A). The cartridge contained a WBC extraction chamber that harbored a Leukosorb filter (Pall Corp) and a flexible membrane that interfaced with an ultrasonic transducer. The extraction chamber had a sweepable volume of ~100 μL. The blood was pumped pneumatically through the filter at a rate of 0.5 mL/min. WBCs were collected on the filter, whereas all other material (i.e., red blood cells and plasma) passed through to a waste chamber. The trapped WBCs were washed with the isotonic solution, and then 200 μL of lysis buffer was pumped into the extraction chamber to displace the isotonic buffer. The WBCs were lysed on the filter by sonication for 15 s at 47 kHz. Lysis buffer (400 μL) was pumped into the extraction chamber, displacing the WBC lysate out to another chamber. The WBC lysate was manually collected and subjected to PCR and CE analysis. Six runs on the cartridge system were performed for each sample and were compared with runs using the QIAamp DNA Blood Mini Kit (Qiagen) as a reference. The cartridge run time was 9 min/sample.

PCR amplification was accomplished on the Smart Cycler (Cepheid) using 25-μL reactions containing 1× *TH01* STR (Fluorescein) primer pair (Promega), 1× STR buffer (Promega), 0.05 U/μL Platinum Taq DNA polymerase (Life Technologies), 1× Smart Cycler additive (0.2 g/L bovine serum albumin, 150 mmol/L trehalose, 2 mL/L Tween 20), and 2.5 μL of WBC lysate obtained from

the cartridge. The thermal cycling conditions were as follows: an initial hold at 90 °C for 30 s; 10 cycles of 94 °C for 60 s, 60 °C for 30 s, and 70 °C for 45 s; 20 cycles of 90 °C for 30 s, 60 °C for 30 s, and 70 for 45 s; and a final hold at 60 °C for 60 s. Because the Smart Cycler exhibited fast ramp rates and precise temperature control, the cycling time was reduced to 55 min compared with 2.5 h on a conventional thermal cycler. CE was accomplished using the P/ACE MDQ system (Beckman) with a fused-silica capillary (ABI) filled with POP4 polymer (ABI) and 10× CE Buffer (ABI). PCR product was injected electrokinetically for 30 s at 5.0 kV. Separation and detection were performed for 15 min at 9.0 kV at 25 °C.

The mean amount of DNA collected from a 200-μL aliquot of blood processed on the cartridge system was 2.24 μg. A WBC extraction efficiency of 51% was calculated based on the relative yield of DNA obtained using the QIAamp Kit. The lower yield was partially attributable to a 25% loss of intact WBCs during storage of the blood (only intact WBCs are trapped by the filter). A

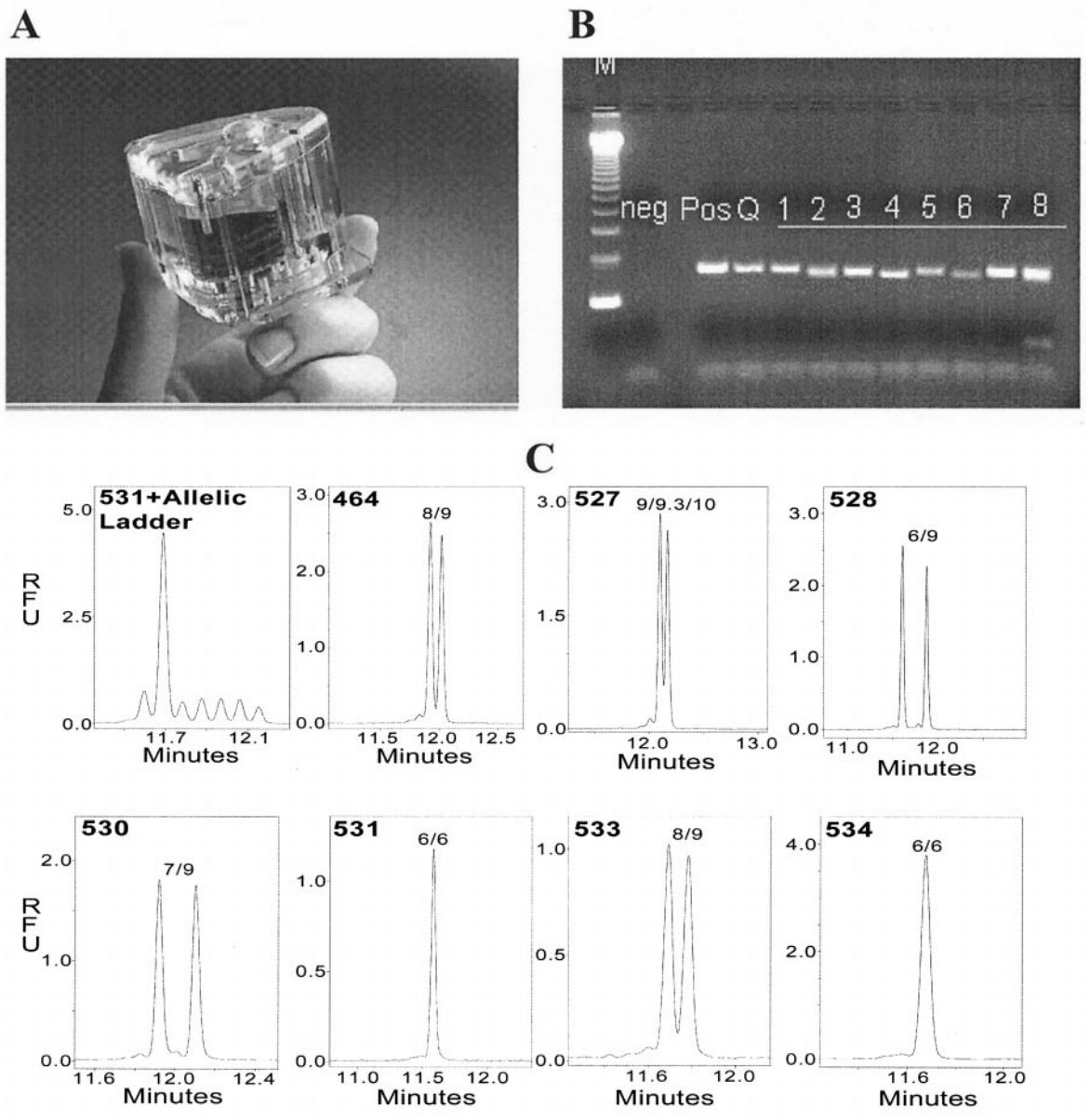

Fig. 1. Microfluidic cartridge for rapidly processing blood for PCR-based genetic testing (*A*), agarose gel electrophoresis of *TH01* STR PCR products (*B*), and STR polymorphism typing of the *TH01* locus using an automated sample preparation cartridge, the Smart Cycler PCR instrument, and the Beckman MDQ CE system (*C*).

(*B*), *lane M*, 123-bp marker; *lane neg*, negative control (no DNA); *lane Pos*, positive control (K562 DNA); *lane Q*, Qiagen method-prepared DNA from individual 527. Cartridge-prepared WBC lysates from individuals 527 (*lane 1*), 528 (*lane 2*), 530 (*lane 3*), 534 (*lane 4*), 533 (*lane 5*), 531 (*lane 6*), 464 (*lane 7*), and 529 (*lane 8*) are shown. (*C*), electropherograms representing seven individual are shown (the coded number assigned to each sample is displayed in the *upper left corner* of each panel). The *TH01* genotype for each individual is indicated *above* the peaks. Sample 531 is shown with and without the allelic ladder. All other samples are shown without the allelic ladder to demonstrate the clean baseline signal. *y-axis*, fluorescence intensity; *x-axis*, migration time (min).

2.5-μL portion of the sample processed on the cartridge system or QIAamp Kit was subjected to PCR to amplify the *TH01* locus. Agarose gel electrophoresis results (Fig. 1B) indicated that the relative yield of PCR products obtained from samples prepared using the two methods were similar.

Allelic typing was performed by adding *TH01* allelic ladder (Promega) to the PCR products generated from the WBC lysates and subjecting the mixtures to CE analysis (Fig. 1C). The ladder ranged in size from 179 to 203 bp and consisted of the alleles designated 5, 6, 7, 8, 9, 9.3/10, and 11. The sharp, distinct *TH01* allelic peaks observed on the electropherograms indicated that robust PCR amplification and CE separation analysis were achieved on the blood samples processed using the cartridge system. The PCR products exhibited a CE migration time of ~13 min. The total time for processing, amplifying, and analyzing the blood sample was 84 min.

In summary, a cartridge system was used to process a 200-μL sample of whole blood in 9 min for genetic testing. This flow-through sample preparation procedure concentrated, extracted, and lysed WBCs from the blood without requiring vortex-mixing, precipitation, and centrifugation. The quantity and quality of DNA from the WBC lysate automatically prepared on the cartridge were sufficient for PCR and CE analysis of the *TH01* STR locus, and the cartridge procedure was at least three times faster than the QIAamp Kit.

References

1. Jin P, Warren ST. Understanding the molecular basis of fragile X syndrome. Hum Mol Genet 2000;9:901–8.
2. Ho LW, Carmichael J, Swartz J, Wyttenbach A, Rankin J, Rubinsztein DC. The molecular biology of Huntington's disease. Psychol Med 2001;31:3–14.
3. Coleman WB, Tsongalis GJ. The role of genomic instability in human carcinogenesis. Anticancer Res 1999;19:4645–64.
4. Bellacosa A, Genuardi M, Anti M, Viel A, Ponz de Leon M. Hereditary nonpolyposis colorectal cancer: review of clinical, molecular genetics, and counseling aspects. Am J Med Genet 1996;62:353–64.
5. Spafford MF, Koch WM, Reed AL, Califano JA, Xu LH, Eisenberger CF, et al. Detection of head and neck squamous cell carcinoma among exfoliated oral mucosal cells by microsatellite analysis. Clin Cancer Res 2001;7:607–12.
6. Simpson AJ, Caballero OL, Pena SD. Microsatellite instability as a tool for the classification of gastric cancer. Trends Mol Med 2001;7:76–80.
7. Steiner G, Reinschmidt G, Muller SC. Molecular genetic diagnosis of de novo and recurrent bladder cancer. Electrophoresis 1999;20:280–2.
8. Balsara BR, Pei J, De Rienzo A, Simon D, Tosolini A, Lu YY, et al. Human hepatocellular carcinoma is characterized by a highly consistent pattern of genomic imbalances, including frequent loss of 16q23.1-24.1. Genes Chromosomes Cancer 2001;30:245–53.
9. Liloglou T, Maloney P, Xinarianos G, Hulbert M, Walshaw MJ, Gosney JR, et al. Cancer-specific genomic instability in bronchial lavage: a molecular tool for lung cancer detection. Cancer Res 2001;61:1624–8.
10. Russo J, Yang X, Hu YF, Bove BA, Huang Y, Silva ID, et al. Biological and molecular basis of human breast cancer. Front Biosci 1998;3:D944–60.
11. Auer RL, Jones C, Mullenbach RA, Syndercombe-Court D, Milligan DW, Fegan CD, Cotter FE. Role for CCG-trinucleotide repeats in the pathogenesis of chronic lymphocytic leukemia. Blood 2001;97:509–15.
12. Fey MF. Microsatellite markers in leukaemia and lymphoma: comments on a timely topic. Leuk Lymphoma 1997;28:11–22.
13. Mori N, Morosetti R, Hoflehner E, Lubbert M, Mizoguchi H, Koeffler HP. Allelic loss in the progression of myelodysplastic syndrome. Cancer Res 2000;60:3039–42.
14. Zhu YM, Das-Gupta EP, Russell NH. Microsatellite instability and p53 mutations are associated with abnormal expression of the MSH2 gene in adult acute leukemia. Blood 1999;94:733–40.
15. Mishra M, Tekwani BL. Removal of leucocytes from malaria-infected blood using leucosorb capsule filter units. Med Sci Res 1996;24:147–8.
16. Puers C, Hammond HA, Jin L, Caskey CT, Schumm JW. Identification of repeat sequence heterogeneity at the polymorphic short tandem repeat locus HUMTH01[AATG]n and reassignment of alleles in population analysis using a locus-specific allelic ladder. Am J Hum Genet 1993;53:953–8.

Fast and Specific Hybridization Using Flow-Through Microarrays on Porous Metal Oxide, *Rinie van Beuningen,* Henk van Damme, Piet Boender, Niek Bastiaensen, Alan Chan, and Tim Kievits* (PamGene B.V., Burgemeester Loeffplein 70a, 5211RX Den Bosch, The Netherlands; * author for correspondence: fax 31-73-615-8081, e-mail RvBeuningen@PamGene.com)

The advent of sequencing technologies and efforts in sequencing and analysis of polymorphic regions in various viruses, bacteria, and higher organisms, including humans, has led to a wealth of genetic information *(1, 2)*. This information is used to relate genetic information to phenotypic effects, which is used to provide better tools in drug development and a better understanding of the biologic pathways involved in various rare as well as common diseases in humans. A tool in this type of analysis is parallel testing on the basis of microarrays. These arrays, sometimes referred to as "DNA-chips", usually consist of a flat surface with capture probes at specific positions (spots) directed toward the various targets that may be present in the sample.

The use of microarrays for genomic-based screening and the search for new genes has been well documented by scientific groups using systems (e.g., from Affymetrix and Sequenom) that have integrated many novel, microscale technologic developments *(3, 4)*. The ability to either deposit directly, or synthesize in situ, hundreds or thousands of oligonucleotides on glass surfaces in subnanoliter volumes at high density allows for high-throughput simultaneous detection.

These first-generation microarrays, characterized by passive hybridization between targets and probes, are typically performed on planar surfaces. The fundamental problem caused by the concept of working on a basic two-dimensional surface has led many research groups to develop second-generation microarrays that seek to enhance the performance of this platform. The aim is more toward low costs, reproducibility of hybridization signals, and speed. The technologies used by these microarrays have properties beyond simple passive hybridization, such as microfabricated fluidic channels, electronic hybridization, novel posthybridization signaling steps, or flow-through dynamics *(5–7)*.

The rate-limiting step in this planar format is the diffusion of the sample molecules (the target) toward the attached probe during hybridization. Because diffusion is slow, incubation usually takes place overnight. To bypass this limitation, we have used a porous aluminum oxide substrate as solid support. The substrate, with a thickness of 60 μm, has long branched capillaries, which are interconnected inside the substrate *(8)*. The diameter of the

individual pores is ~200 nm. The interstitial volume inside the material is only 30 nL/mm^2. Compared with a flat two-dimensional surface, the reactive surface in this material is increased 500-fold. In addition, the permeable nature of the microarray facilitates the pressurized movement of fluid, such as the sample solution, through its structure. In contrast to flat, solid-surface arrays, the flow-through microarray substantially reduces hybridization times and increases signal and signal-to-noise ratios.

The flow-through microarrays can be prepared with, for example, an array of oligonucleotides. We used a noncontact inkjet-spotting technique to deposit and covalently link an array of oligonucleotides onto the substrate. The inkjet technology enables accurate spotting of 325 pL in single droplets with a distance of 0.2 mm between the centers of each spot *(9)*.

To show hybridization stringency and speed of this new three-dimensional porous substrate, we prepared an 18-oligonucleotide array that contains several single and multiple mismatches. A fluorescently labeled oligonucleotide was used as a sample and incubated at various temperatures while the solution was pumped, twice per minute, through the substrate; the amount of bound target fluorescent oligonucleotide after each pumping step was detected by a charge-coupled device (CCD)-equipped epifluorescence microscope.

The flow-through microarray was made of activated 1 × 4 cm aluminum oxide substrate (Whatman). This substrate was placed between two sheets of pressure-sensitive adhesive foil (2.5 × 7.6 cm), each containing four aligned holes 4 mm in diameter on a pitch distance of 9 mm. These openings, called arrays, enable access to the aluminum oxide substrate. A set of 21mer oligonucleotides (Isogen) was synthesized (Table 1) and spotted in 325-pL droplets, containing 0.1 mmol/L of the oligonucleotide mixture, on the arrays with a Packard BioChip Arrayer (Meriden). The foil containing the oligonucleotide arrays was used in a reusable anodized aluminum holder (PamGene) that had four wells that matched the arrays on the foil. A water bath was coupled to an inlet and an outlet on the holder to control the reaction temperature. O-rings were used in the aluminum holder to eliminate crossover between each of the arrays. A syringe pump (Hamilton) was attached to the wells of the aluminum holder. This allowed increased or decreased pressure to be applied to the arrays to pump the sample solution twice per minute across the substrate at a flow rate of 25 μL/15 s.

A 25-μL sample containing 10 nmol/L 5′-fluorescein-labeled oligonucleotide (Isogen) in phosphate-buffered saline (NPBI) was added to a well of the aluminum holder and pumped twice per minute across the substrate.

After each pumping step, the fluorescence was recorded by an epifluorescence microscope (Olympus) and digitized with a CCD camera (Sony). The image information was converted into spot intensity values by a MatLab software image analysis package (PamGene).

The limit of detection of the epifluorescence CCD microscope system was ~5 × 10^6 fluorescent molecules per spot with a two-log dynamic range when an 8-bit CCD camera was used.

The fluorescent oligonucleotide target was rapidly bound inside the interconnected pores of the substrate by the applied pressure difference of 10 000 Pa, which allows the sample to pass through the substrate twice per minute (Fig. 1A).

The hybridization results after 0, 1, 2, 9, 16, 31, 38, 44, 50, and 55 min are shown in Fig. 1A. The signal increased from 0 to 31 min. The specificity of the binding was determined by changing the hybridization stringency at

Table 1. Sequences of the 21mer oligonucleotides.[a]

Probe	T	T	G	T	A	C	A	G	A	A	A	T	G	G	A	A	A	A	G	G	A	Mismatches
A	–	–	–	–	–	–	–	–	–	–	–	–	–	–	–	–	–	–	–	–	–	0
B	–	–	–	–	G	–	–	–	–	G	–	–	–	–	–	–	–	–	–	–	–	2
C	–	–	–	–	–	A	–	–	–	–	–	–	–	–	–	–	C	–	–	–	–	2
D, neg. control	Unrelated sequence																					
E	–	–	–	C	–	–	–	–	–	–	–	–	–	–	–	–	–	–	–	–	–	1
F, Fl. control	Unrelated sequence																					
G	–	–	–	–	–	–	–	–	–	–	C	–	–	–	–	–	–	–	–	–	–	1
H	–	–	–	–	T	T	–	–	–	–	–	–	–	–	–	–	–	–	–	–	–	2
I	–	–	–	–	G	–	–	T	T	T	–	–	–	–	–	G	G	–	–	–	–	6
J	–	–	–	–	G	–	–	–	–	–	–	–	–	–	–	–	–	–	–	–	–	1
K	–	–	–	–	–	–	–	–	–	–	–	–	C	–	–	–	–	–	–	–	–	1
L	C	C	A	–	T	G	–	C	–	G	–	A	–	A	–	–	–	–	A	T	–	11
M	–	–	A	A	T	A	–	–	–	G	–	A	C	T	C	–	–	G	A	C	T	13
N	–	–	–	–	–	A	–	–	–	G	–	–	–	–	–	–	C	–	–	–	–	3
O	–	–	–	–	–	–	–	–	–	G	–	–	–	–	–	–	–	–	–	–	–	1
P	–	–	–	–	–	–	–	–	–	–	–	–	–	–	–	G	–	–	–	–	–	1
Q	–	–	–	–	–	–	–	–	–	–	C	–	–	–	–	G	–	–	–	–	–	2
R	–	–	–	–	–	–	–	–	–	–	T	–	–	–	–	–	–	–	–	–	–	1

[a] Both D, the negative control, and F, the fluorescence-positive control, are sequences unrelated to the target. The positive control is used to focus the fluorescence microscope.

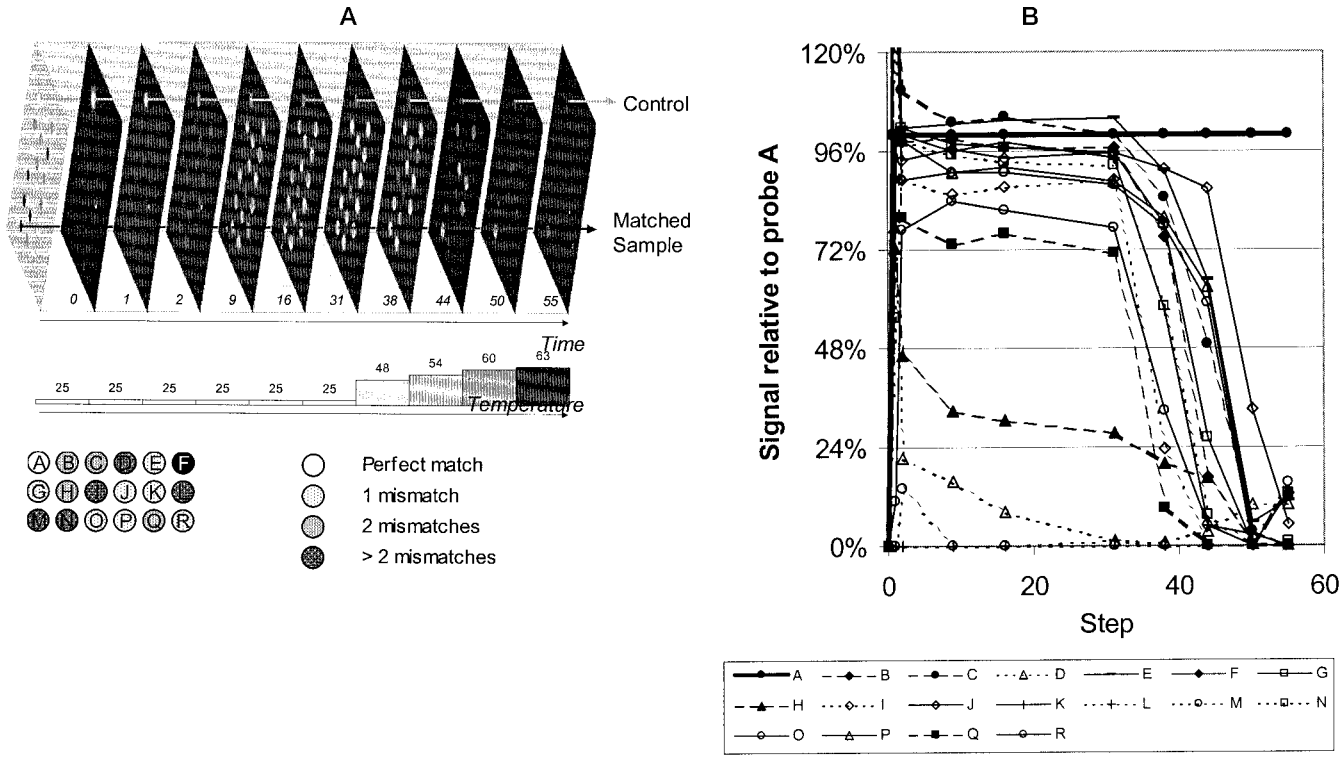

Fig. 1. Schematic of the movement of oligonucleotides through the array (*A*) and signal intensities of probes (*B*).

(*A*), the setup of the array is shown at the *bottom*. The sequences are outlined in the text. The hybridization results are shown after 0, 1, 2, 9, 16, 31, 38, 44, 50, and 55 min. The *Control* (*spot F*) is a fluorescent oligonucleotide used for focusing of the array. At 38, 44, 50, and 55 min, the temperature of the hybridization was changed to 48, 54, 60, and 63 °C, respectively. (*B*), signal intensities for *probes B–R* compared with the perfectly matching *probe A*.

38, 44, 50, and 55 min. This was achieved by adjusting the temperatures from 25 °C, thus increasing the hybridization stringency to 48, 54, 60, and 63 °C, respectively. The end result was a specific hybridization with a single specific spot on the array (Fig. 1A).

A comparison of the signal intensity values of the perfectly matched spot A compared with spots B–R is shown in Fig. 1B. Increasing the temperature to 48 °C and higher increased the specificity and therefore the signal difference between the perfect match and single or multiple mismatches. At 63 °C, the signal of the perfect match was discriminated from all other single mismatches by a factor of four.

The flow-through aluminum oxide matrix with its interconnecting pores offers many features that are not found on existing silica or membranous microarrays. This three-dimensional structure enables real-time hybridization kinetics, which until recently were associated only with platforms such as spectrophotometry or surface plasmon resonance (Biacore). This technology is scalable and enables parallel analysis of many hundreds of samples on many hundreds of different nucleic acid sequences while using a temperature profile to ensure the highest specificity. This second-generation microarray format will address part of the challenge to provide tools for clinical diagnostics and life science research.

References

1. Venter JC, Adams MD, Myers EW, Li PW, Mural RJ, Sutton GG, et al. The sequence of the human genome. Science 2001;291:1304–51.
2. Lander ES, Linton LM, Birren B, Nusbaum C, Zody MC, Baldwin J, et al. Initial sequencing and analysis of the human genome. Nature 2001;409:860–921.
3. Wikman FP, Lu ML, Thykjaer T, Olesen SH, Andersen LD, Cordon-Cardo C, Orntoft TF. Evaluation of the performance of a p53 sequencing microarray chip using 140 previously sequenced bladder tumor samples. Clin Chem 2000;46:1555–61.
4. Fu DJ, Tang K, Braun A, Reuter D, Darnhofer-Demar B, Little DP, et al. Sequencing exons 5 to 8 of the p53 gene by MALDI-TOF mass spectrometry. Nat Biotechnol 1998;16:381–4.
5. Sassi AP, Paulus A, Cruzado ID, Bjornson T, Hooper HH. Rapid, parallel separations of d1S80 alleles in a plastic microchannel chip. J Chromatogr A 2000;894:203–17.
6. Sosnowski RG, Tu E, Butler WF, O'Connell JP, Heller MJ. Rapid determination of single base mismatch mutations in DNA hybrids by direct electric field control. Proc Natl Acad Sci U S A 1997;94:1119–23.
7. Steel A, Torres M, Hartwell J, Yu Y-Y, Ting N, Hoke G, Yang H. The Flow-thru Chip™: a three-dimensional biochip platform. In: Schena M, ed. DNA microarrays: biology and technology. Natick, MA: BioTechniques Books, 2000:87–114.
8. Rigby WR, Cowieson DR, Davies NC, Furneaux RC. An anodizing process for the production of inorganic microfiltration membranes. Trans Inst Met Finish 1990;68:95–8.
9. Bateman TA, Ayers RA, Greenway RB. An engineering evaluation of four fluid transfer devices for automated 384-well high throughput screening. Lab Robotics Automation 1999;11:250–9.